

Do radiative forcings of methane and ozone cancel out? - A case study from the last IMO Greenhouse gas study

Jérôme Hilaire^{*}, Ruben Rodriguez de Leon, David S. Lee
Dalton Research Institute, Manchester Metropolitan University, UK

Keywords: Shipping, NO_x emissions, Atmospheric composition, Climate impacts, IMO GHG Study 2, MOZART-2, GCTM, Edwards&Slingo, RTM.

ABSTRACT: This modelling work aims at quantifying the perturbation resulting from international maritime transport emissions of nitrogen oxides on the lower atmospheric composition and radiative forcing. We use the emission dataset created for the new IMO Greenhouse gas study as input to the tropospheric GCTM MOZART-2. We further run the Edwards & Slingo Radiative Transfer Model to assess impacts on the radiative forcing. The IMO emissions of nitrogen oxides are large compared to previous assessments (about 8Tg(N).yr⁻¹ in this study, compared to about 4Tg(N).yr⁻¹ before). These emissions cause significant perturbations in ozone (35mW.m⁻²) and methane (-45mW.m⁻²) which in turn result in a significant radiative forcing. However, it is likely that these impacts are overestimated because the non-linearity introduced by subgrid scale plume processes that are not accounted.

1 INTRODUCTION

International shipping is undeniably a cornerstone of the global economy. However, it is an increasing environmental problem that consumes large quantities of fossil fuel and releases significant amounts of atmospheric pollutants leading to acidification, eutrophication, premature mortality [Corbett *et al.*, 2007] and climate change. In addition, the CO₂ emissions from international shipping (the largest fraction) are not covered under the Kyoto Protocol (Article 2.2).

Indeed, by emitting nitrogen oxides (NO_x), carbon monoxide (CO) and volatile organic compounds (VOCs) in the marine boundary layer and through complex chemical processes, these molecules contribute to the formation of ozone (O₃) and the depletion of methane (CH₄) which induce climate change.

Several studies [Corbett *et al.*, 2001], [Endresen *et al.*, 2003], [Eyring *et al.*, 2005], [Eyring *et al.*, 2009] have presented different values resulting from a large range of shipping emissions. However, all patterns look similar.

This study focuses on the trade-off between impacts of ozone and methane on the climate stemming from a shipping perturbation induced by emissions calculated for IMO [Buhaug, *et al.*, 2009]. First, the methodology is presented, the results from the simulations are discussed and finally, conclusions are drawn.

2 METHODOLOGY

In order to carry this research, shipping emissions are provided to a Global Chemistry-Transport Model (MOZART-2 [Horowitz *et al.*, 2003]). MOZART-2 is a tropospheric chemical transport model accounting for the most important processes occurring in the lowermost part of the atmosphere. This version of the model calculates the global distribution of 63 gas-phase chemical species over a T63 (roughly equivalent to 1.875° × 1.875°) grid and 47 hybrid vertical levels ranging from the surface to about 10 hPa. In addition, the model time step for chemistry and transport is set to 15

^{*} *Corresponding author:* Jérôme Hilaire, PhD Student, Dalton Research Institute, MMU, UK. Email: j.hilaire@mmu.ac.uk

minutes. The dynamical meteorological data are provided from the ECMWF Operational Analysis data for 2003. Chemical species are transported by several physical processes. Advection is performed using a flux-form semi-Lagrangian scheme [Lin and Rood, 1996] with a pressure fixer. Vertical diffusion is treated with the Holstag and Boville parametrization [Holtslag and Boville, 1993] and convection is split into two schemes: deep convection [Hack, 1994] and shallow convection [Zhang and McFarlane, 1995]. Dry and wet deposition is parameterised in the model. Stratospheric concentrations of 7 long-lived species are constrained by relaxation toward climatological values. Details on the treatment of the gas-phase chemical mechanisms and transport processes are described by [Horowitz et al, 2003].

The perturbed chemical species values constitute then an input to a Radiative Transfer Model (RTM) (Edwards & Slingo [Edwards and Slingo, 1996]) that estimates the change in the Earth's radiative balance and thus the impact on climate. The Edwards & Slingo RTM has been tested over a significant number of studies. Radiative fluxes are performed using the δ -Eddington form of the two-stream equations in both the short-wave and long-wave regions of the spectrum.

This study makes use of the emission dataset created for the new IMO Greenhouse study [Buhaug et al, 2008-2009]. Two 1-year spin-up simulations are run, one with the IMO emissions and the other one without. After this, two new simulations are started but this time with initial conditions provided by the spin-up simulations.

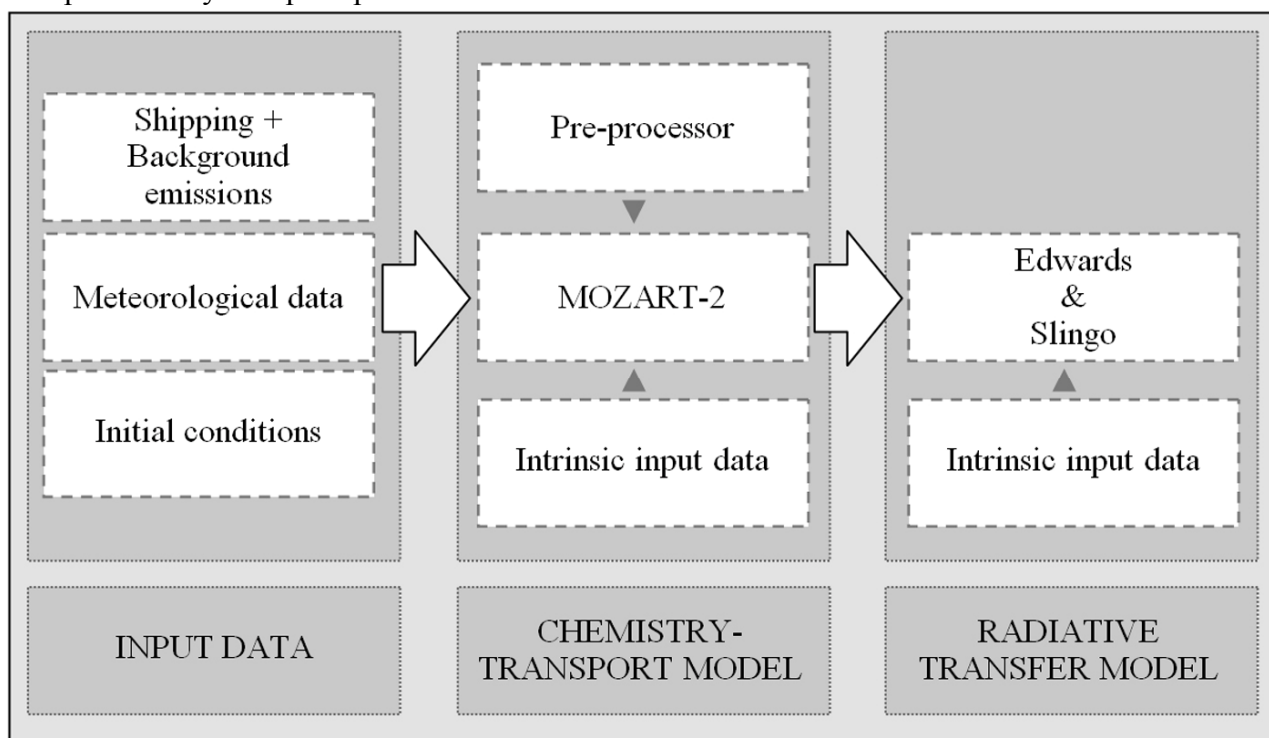


Fig 2.1 – Schema of modelling system

3 IMPACTS ON ATMOSPHERIC COMPOSITION AND RADIATIVE FORCING

In this case study, emissions from the recent IMO Greenhouse gas study are employed. These emissions are larger than estimated in previous studies. For instance, NO_x emissions are 7.3 Tg(N)/yr which is almost twice the amount of nitrogen oxides used in the past (eg 3.10 in [Eyring et al, 2007], 4.38 in [Fuglestedt et al, 2008]). Emissions of VOCs are also larger than previous estimations (see **Fig 3.1**). Shipping NO_x emissions correspond to about 15% of the total anthropogenic NO_x emissions. Background emissions are from the GEMS study [Schultz and Stein, 2006]. Emission totals of CH_4 and NO_x , are in good agreement with the Fourth assessment report from the IPCC [cf Chapter 7]. Whereas spin-up simulations are run with prescribed methane lower-boundary concentrations, the following simulations account for CH_4 emissions (516 Tg(CH_4)/yr).

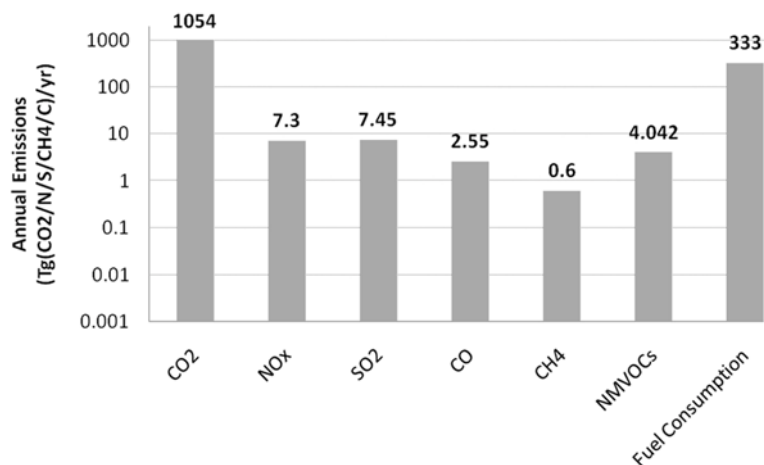
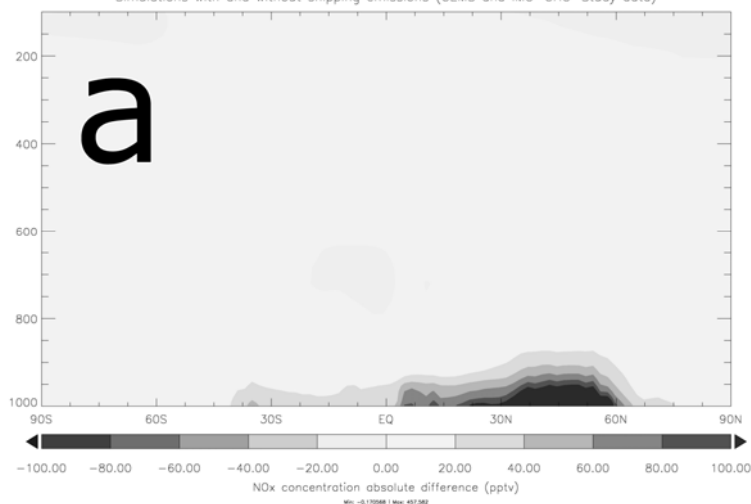


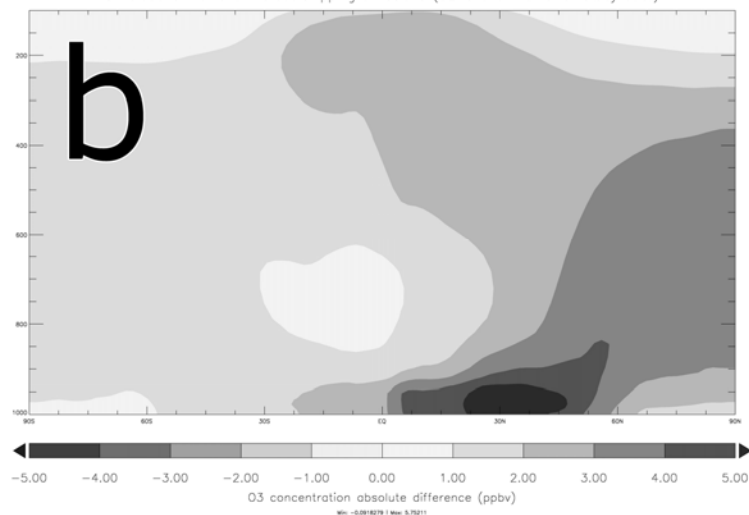
Fig 3.1 – Annual total shipping emissions for different chemical species. [Source: IMO GHG Study 2009]

The magnitude of the ozone shipping perturbation resulting from the difference between the 2 simulations is consistent with previous studies [Eyring et al, 2007] when differences in NO_x emissions are accounted for. The pattern is also in good agreement (see Fig 3.2). However, the impact on the methane lifetime is larger and quite significant. Indeed, according to the model, it could be reduced by about 0.9 year. This means that once methane would reach steady state it could have been globally reduced by more than 250 ppbv. Even though this value is large compared with the ones presented in a recent assessment of shipping impacts [Eyring et al, 2009], it still belongs to the range of magnitude.

Annually & Longitudinally averaged Latitude/Sigma–Pressure plots of ΔNO_x concentrations
Simulations with and without shipping emissions (GEMS and IMO–GHG–Study data)



Annually & Longitudinally averaged Latitude/Sigma–Pressure plots of ΔO₃ concentrations
Simulations with and without shipping emissions (GEMS and IMO–GHG–Study data)



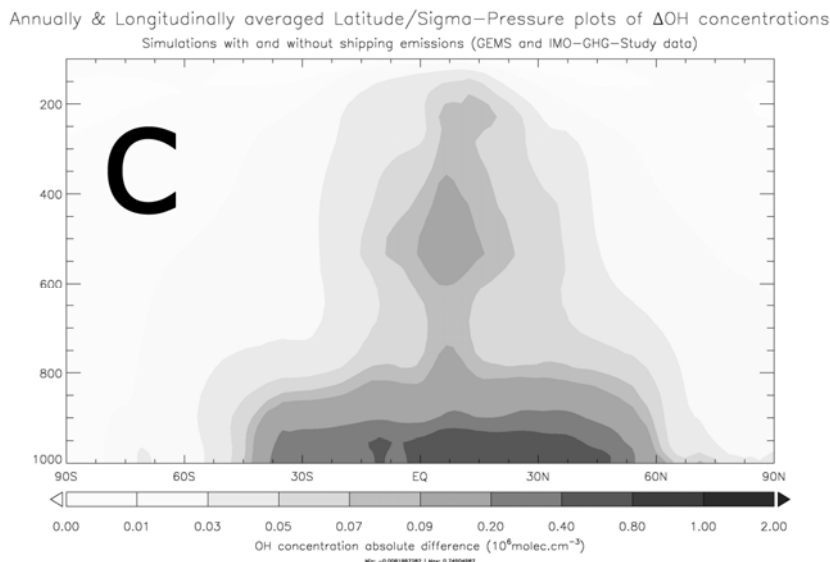


Fig 3.2 – Annual and longitudinal average of atmospheric chemical species. a. nitrogen oxides – b. ozone – c. hydroxyl radical

Table 3.1 – Annually averaged methane lifetimes

Simulation	Methane lifetime
1. With shipping emissions	9.48
2. Without shipping emission	10.4
Difference between simulations (1 – 2)	-0.92

Because of the formation of ozone and the depletion of methane due to emissions of nitrogen oxides, the radiative forcing from shipping ozone is positive whereas the radiative forcing of shipping methane is negative.

Using LinClim [Lim et al, 2005] to normalize the results, we find a global radiative forcing from ozone of $35 \text{ mW}\cdot\text{m}^{-2}$ and radiative forcing from methane is $-45 \text{ mW}\cdot\text{m}^{-2}$. The sum of these 2 components results in a small negative value. However, although, these radiative forcings operate on similar latitudinal scales, but they also present some variability ranging from $0.02 \text{ mW}\cdot\text{m}^{-2}$ in the northern tropical and the southern polar regions to $-20 \text{ mW}\cdot\text{m}^{-2}$ near the southern tropic (see Fig 3.3).

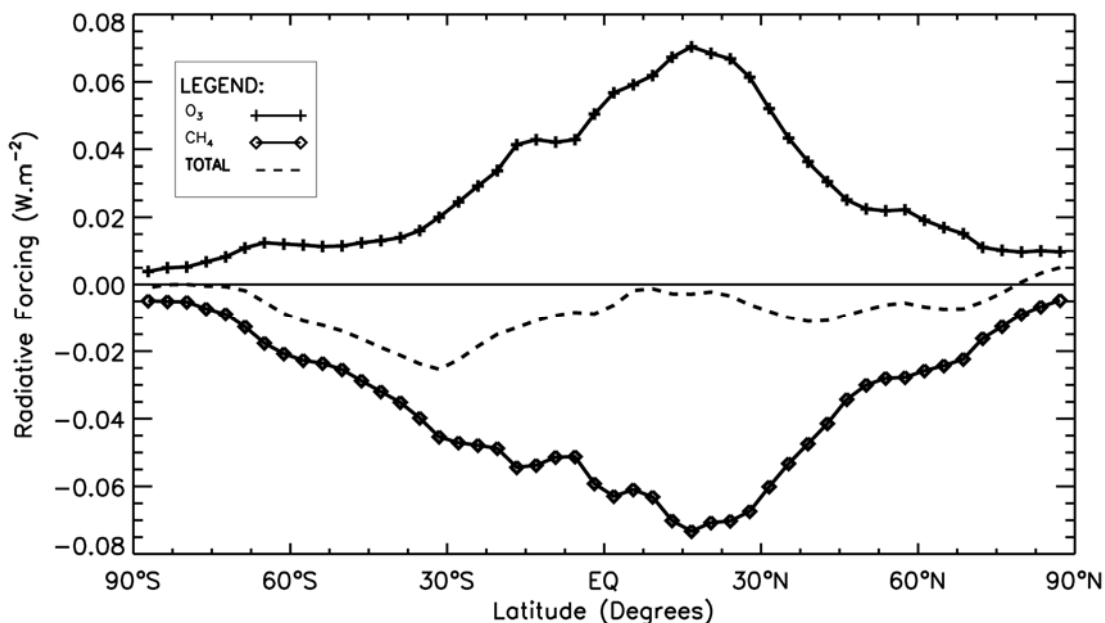


Fig 3.3 – Annual radiative forcing from total shipping in 2007.

4 CONCLUSIONS AND PERSPECTIVES

The magnitudes of the ozone and methane perturbations are larger than previous studies but they scale linearly to the emitted NO_x (about 2 times higher). However the methane lifetime perturbation is at the higher end of the range of values of previous studies. Although the radiative forcings of ozone and methane are globally of the same order of magnitude, the latitudinal plot (**Fig 3.3**) shows some variability which can be significant depending on the location. As a consequence, these radiative forcings do not necessarily cancel out regarding position (a map would give more details).

Also, a subgrid scale parameterisation would probably reduce errors inherent to coarse resolution modelling [Franke et al, 2007], [Cariolle et al, 2009].

It would be interesting to look at the whole set of radiatively active components in the future to foresee the impacts of shipping.

Implementing the recent findings on halogen-mediated ozone destruction in the model could also give a different atmospheric composition. And especially, it could lead to another ozone perturbation. [Read et al, 2008]

REFERENCES

- Buhaug, Ø., J.J. Corbett, Ø. Endresen, V. Eyring, J. Faber, S. Hanayama, D.S. Lee, D. Lee, H. Lindstad, A.Z. Markowska, A. Mjelde, D. Nelissen, J. Nilsen, C. Palsson, J.J. Winebrake, W.-Q. Wu and K. Yoshida, 2009: Second IMO GHG study; International Maritime Organization (IMO) London, UK
- Corbett, J. J. and J.J. Winebrake, 2003: Updated emissions from ocean shipping
- Corbett, J. J., J.J. Winebrake, E.H. Green, P. Kasibhatla, V. Eyring and A. Lauer, 2007: Mortality from Ship Emissions: A Global Assessment
- Cariolle, D., D. Caro, R. Paoli, D.A. Hauglustaine, B. Cuenot, A. Cozic and R. Paugam, 2009: Parametrization of plume chemistry into large-scale atmospheric models: application to aircraft NO_x emissions [*in preparation*]
- Edwards, J. M and Slingo, A., 1996: Studies with a flexible new radiation code. I: Choosing a configuration for a large-scale model
- Endresen, Ø., E. Sørsgard, J.K. Sundet, S.B. Dalsoren, I.S.A. Isaksen, T.F. Berglen and G. Gravir, 2003: Emission from international sea transportation and environmental impact
- Eyring, V., H.W. Kohler, J. van Ardenne and A. Lauer, 2005: Emissions from international shipping 1. Past 50 years
- Eyring, V., D.S. Stevenson, A. Lauer, F.J. Dentener, T. Butler, W.J. Collins, K. Ellingsen, M. Gauss, D.A. Hauglustaine, I.S.A. Isaksen, M.G. Lawrence, A. Richter, J.M. Rodriguez, M. Sanderson, S.E. Strahan, K. Sudo, S. Szopa, T.P.C. van Noije and O. Wild, 2007: Multi-model simulations of the impact of international shipping on Atmospheric Chemistry and Climate in 2000 and 2030
- Eyring, V., I.S.A. Isaksen, T. Bernsten, W.J. Collins, J.J. Corbett, Ø. Endresen, R.G. Grainger, J. Moldanova, H. Schlager and D.S. Stevenson, 2009: Transport impacts on atmosphere and climate: Shipping
- Franke, K., V. Eyring, R. Sander, J. Hendricks, A. Lauer and R. Sausen, 2007: Towards Effective Emissions of Ships in Global Models
- Fuglestvedt, J., T.K. Bernsten, I.S.A. Isaksen, H. Mao, X.-Z. Liang, and W.-C. Wang, 1999: Climatic forcing of nitrogen oxides through changes in tropospheric ozone and methane; global 3D model studies
- Horowitz, L. W., S. Walters, D.L. Mauzerall, L.K. Emmons, P.J. Rash, C. Granier, X. Tie, J.-F. Lamarque, M.G. Schultz, G.S. Tyndall, J.J. Orlando and G.P. Brasseur, 2003: A global simulation of tropospheric ozone and related tracers: Description and evaluation of MOZART, version 2
- Lim, L. L., D.S. Lee, R. Sausen and M. Ponater, 2005: Calculating radiative forcing and temperature changes from aviation effects with a climate response model
- Read, K., A.S. Mahajan, L.J. Carpenter, M.J. Evans, B.V.E. Faria, D.E. Heard, J.R. Hopkins, J.D. Lee, S.J. Moller, A.C. Lewis, L. Mendes, J.B. McQuaid, H. Oetjen, A. Saiz-Lopez, M.J. Pilling and J.M.C. Plane, 2008: Extensive halogen-mediated ozone destruction over the tropical Atlantic Ocean
- Schultz, M. G. and Stein, O., 2006: GEMS (GRG) Emissions for 2003 reanalysis simulations. Technical report, MPI-M Hamburg, 2006

Aerosol optical properties

D.M. Peters*, R.G. Grainger, G. Thomas

Sub-Department of Atmospheric, Oceanic and Planetary Physics, University of Oxford, UK

Keywords: aerosol optical properties, aerosol refractive index

ABSTRACT: Traditionally the atmospheric physics department at the University of Oxford has applied optimal estimation techniques for the retrieval of atmospheric properties of gases; temperature, pressure and volume mixing ratio from satellite measurements. This paper describes the latest novel application of these techniques in deriving aerosol optical properties in laboratory experiments. Two examples are given; a spectral resolved technique allows an aerosol refractive index to be derived over a wide wavelength range and a method of deriving single particle refractive index and size from a novel aerosol instrument suitable for in situ aerosol monitoring.

1 OPTIMAL ESTIMATION; A GENERIC METHOD

Optimal estimation has a long history in use in remote sensing. The advantage over other methods is the ability to provide the highest information content for a retrieval problem. This is achieved by using a model that contains all the known physics of the problem and prior knowledge of the measurement. In addition the method provides error estimates on the parameter(s) of interest. The following paragraphs provide a quick overview of the method; for a detailed discussion of the method refer to Rodgers (2000).

Measurement(s), \mathbf{y} are related to the state, \mathbf{x} by physics. This is represented by the forward model, $\mathbf{F}(\mathbf{x})$. Hence the relationship of the state to measurement can be described by the equation:

$$\mathbf{y} = \mathbf{F}(\mathbf{x}) \quad (1)$$

We need to invert our measurements to find the state, \mathbf{x} (i.e. refractive index, and particle size in the examples to follow). We also use the best knowledge of the solution, \mathbf{x}_a before the measurement was made, thus the problem is to solve the inverse model:

$$\mathbf{x} = \mathbf{F}^{-1}(\mathbf{y}, \mathbf{x}_a) \quad (2)$$

To do this we minimise the cost function Φ , to find the state \mathbf{x} :

$$\Phi(\mathbf{x}) = (\mathbf{x} - \mathbf{x}_a)^T \mathbf{S}_{x_a} (\mathbf{x} - \mathbf{x}_a) + (\mathbf{y} - \mathbf{F}(\mathbf{x}))^T \mathbf{S}_y^{-1} (\mathbf{y} - \mathbf{F}(\mathbf{x})) \quad (3)$$

And we find our estimated state, $\hat{\mathbf{x}}$ is given by:

$$\hat{\mathbf{x}} = \mathbf{x}_a + \mathbf{S}_{x_a} \mathbf{K}_x^T \mathbf{S}_y^{-1} (\mathbf{y} - \mathbf{F}(\hat{\mathbf{x}})) \quad (4)$$

Where the weighting function \mathbf{K}_x is:

$$\mathbf{K}_x = \frac{\partial \mathbf{F}}{\partial \mathbf{x}} \quad (5)$$

Equation 4 and 5 are generally by the Levenberg-Marquardt algorithm (Gauss-Newton and the gradient descent iteration methods). For details of how the uncertainty estimates are calculated see Rodgers (2000).

* *Corresponding author:* Dr Daniel Peters, University of Oxford, AOPP, Clarendon laboratory, South parks road, OX1 3PU, UK. Email: dpeters@atm.ox.ac.uk

2 AEROSOL REFRACTIVE INDEX

The following section shows the application of this optimal estimation to determining the spectrally dependent refractive index of aerosols in a test cell.

2.1 Method

The extinction cross section of an aerosol in the cell is related to the optical transmission by:

$$T(\lambda) = e^{-\beta(\lambda)x} \quad (6)$$

Where, $T(\lambda)$ is the transmission, $\beta(\lambda)$ the volume extinction coefficient, x path length though the test cell at the wavelength λ . The extinction coefficient can be calculated if we assume Mie theory and know the particle size distribution from the equation:

$$\beta(\lambda) = \int_0^{\infty} \sigma_{ext}(r, m(\lambda), \lambda) n(r) dr \quad (7)$$

Where, σ_{ext} is the extinction coefficient (assuming Mie theory), r is the particle radius, $m(\lambda)$ the refractive index and $n(r)dr$ the number of particles between radii r and $r + dr$.

In this application of the optimal estimation method the forward model $\mathbf{F}(\mathbf{x})$ represents equations 6 and 7, with the state vector, \mathbf{x} containing the size distribution and refractive index. The measurement vector \mathbf{y} contains the spectrally resolved transmission measurement.

Experimental setup Figure outlines the basic configuration of the experiments undertaken. The aerosol is generated (the method is chosen based on the aerosol type) and the aerosol introduced to aerosol test cell. The aerosol cell has optical windows fitted, allowing the aerosol absorption to be measured via the Fourier Transform Spectrometer, FTS. Particle size distribution of the aerosol is then determined using techniques insensitive to particle refractive index and the aerosol vented into a fume cupboard. The configuration also included a water bath to allow the relative humidity to be controlled.

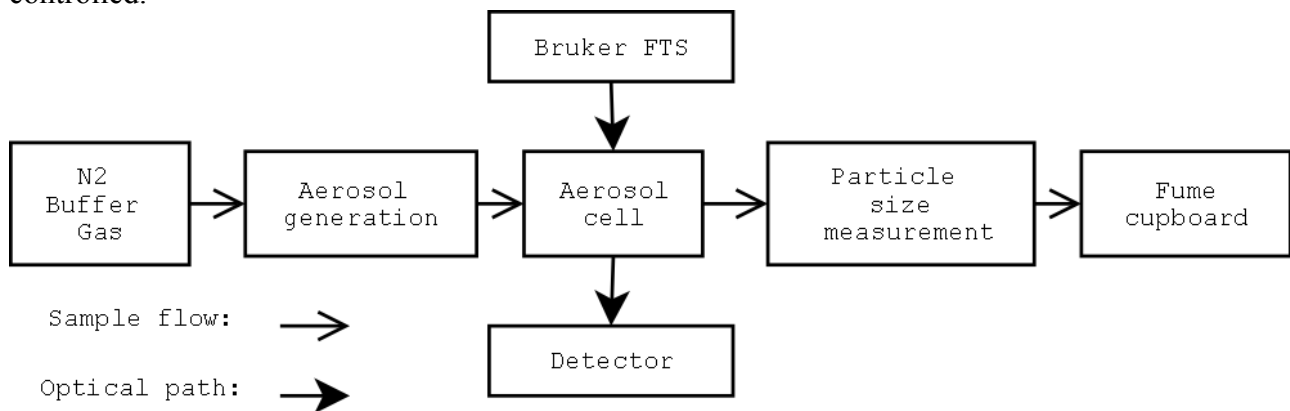


Figure 1. Simplified diagram of experimental configuration.

All of the measurements were undertaken at the Molecular spectroscopy facility at the Rutherford Appleton laboratory, a UK NERC funded facility. The aerosol cell used has an optical path length of 30 cm. Future work is planned to use a multi-pass cell to look at black carbon aerosol optical properties. Spectral intensity measurements are made using a Bruker FTS. Measurements of the detected spectrum are obtained with and without the aerosol to calculate the transmission spectrum, $T(\lambda)$. The method has been described in detail by Thomas (2005). A correction is made to the transmission spectrum to remove water and carbon-dioxide gas absorption lines; this was achieved via a separate retrieval of these gas species concentrations.

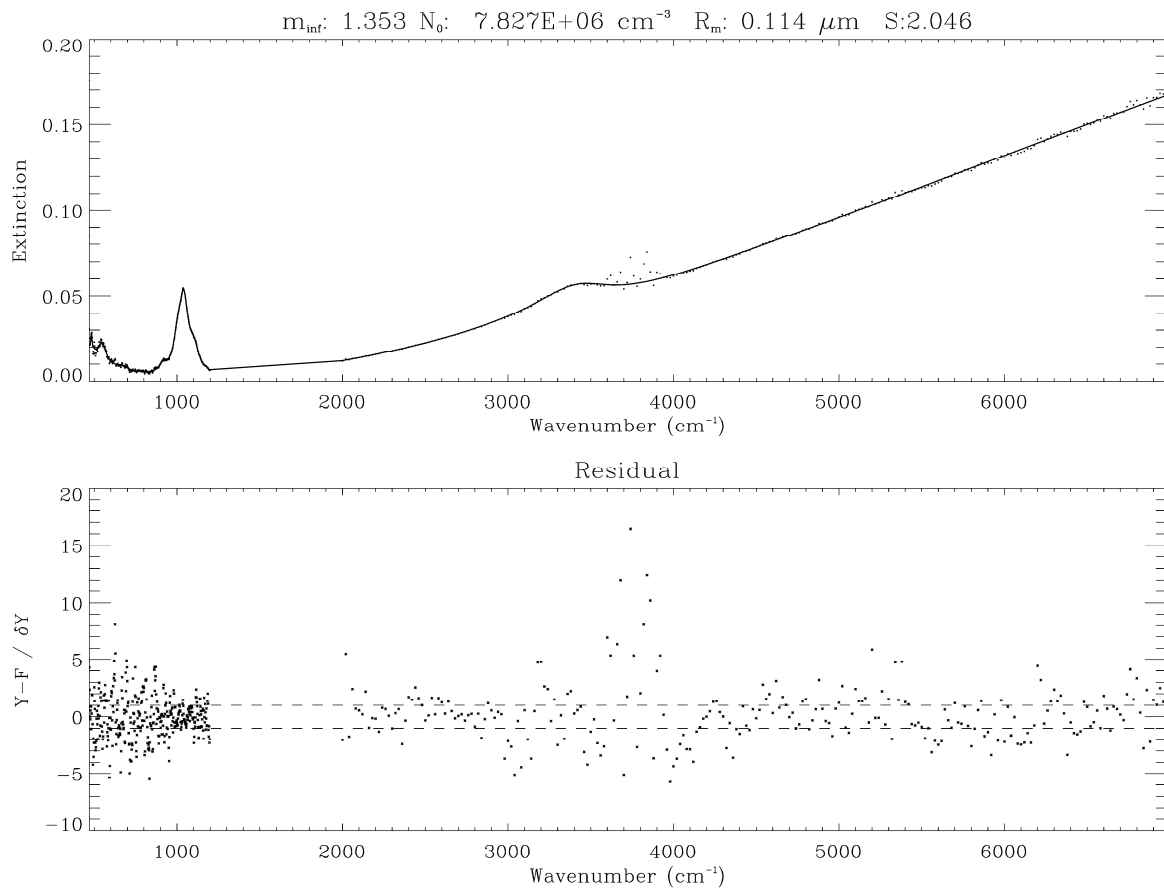


Figure 2. Top plot: Measured spectra (dots) and fitted spectra (lines). Bottom plot: fitted residual.

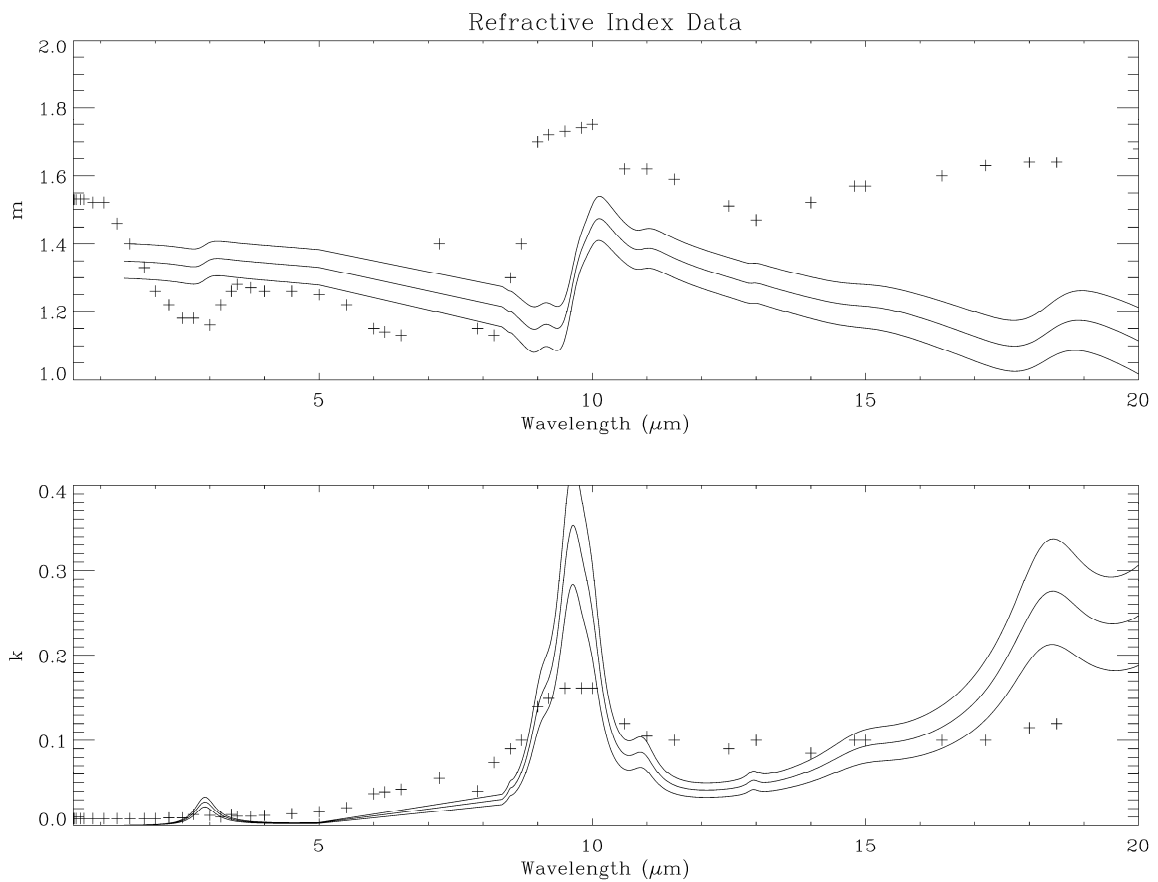


Figure 3. Inverted complex refractive example for Cape Verde dust (central black line). Surrounding two black lines indicates estimated uncertainties. Crosses show the existing published data [2]. Note these are still preliminary results.

2.2 Results

The refractive index of the aerosol from the measured absorption spectra has been determined using this method. This is the first time that the spectral dependent refractive index has been measured on a real mineral aerosol in the laboratory, past measurements are based on collected samples pressed into KBr pellets, for example Shettle (1979). An example of the measurement and forward model fit is shown in Figure , the associated refractive index in Figure . These are preliminary results; the final results may differ and will be published after further validation work. Further results have been published using this method by Irshad (2009) for sea salt aerosols.

3 A NOVEL INSTRUMENT

The angular scattering of radiation by a particle is not only dependent on its size and shape, but also on its refractive index. Traditionally, this dependence has been viewed as a hindrance to the performance of optical particle counters, as it requires assumptions to be made about the refractive index to allow size estimates to be calculated. Instruments such as the Wyoming OPC use white light and carefully positioned detectors to minimize the sensitivity of the instrument to particle refractive index (Dashler 2003). The SPARCLE instrument represents a shift in measurement principle to actively using this dependence to gain more information about the aerosol particles. Additionally, data analysis is performed on a particle-by-particle basis in the SPARCLE system. This enables the attribution of particles' sources (by their refractive index) to different size ranges this cannot be done using the Wyoming OPC system, where the returned data are simply the number of counts per channel.

3.1 Method

There are two key innovations that form the basis of the SPARCLE instrument. Firstly the use of a solid state detector array within a small, autonomous in situ instrument to provide a high resolution measurement of particle scattering on single particles. Secondly the analysis scheme employed by the instrument is completely original. This is to our knowledge the first numerical retrieval scheme which provides both the particle radius and the complex refractive index from a measurement of light in the Mie scattering regime. The development of such an algorithm and its application to actual measurements represents a new state-of-the-art in optical particle measurement.

Sensitivity to both refractive index and size allows measurement of the single scatter albedo on each particle (by assuming Mie theory). This is a significant advantage as SPARCLE is the first instrument to be able to make this measurement on single particles in the atmosphere.

3.2 Results

The instrument uses two detectors; a fast sensitive photomultiplier tube (PMT) and a linear detector array (LDA). The LDA records individual particle phase functions and the PMT measures over a wide angular range to provide sensitivity to the smallest particles. Thus the forward model; $\mathbf{F}(\mathbf{x})$ relates the detectors measured phase function via mie theory to the particle size and refractive index, the state vector \mathbf{x} . The optimal position of the detectors has been determined by calculation of the number of degrees of freedom to allow the highest instrument performance to be obtained i.e. the best ability to distinguish size and refractive index. The Figure demonstrates that real part of the refractive index and particle size are obtainable up to a lower size limit of around $0.1\mu\text{m}$ in radius. The real and imaginary parts of the refractive index and the particle size are available for particles sizes of $0.2\mu\text{m}$ in radius and above.

The current prototype instrument is able to detect and measure the phase function of test particles and has been field tested. Further work is required to increase the LDA sensitivity. The current set up is limited by digitization noise. Low noise pre-amplification is required to ensure the detectors are dark current limited hence obtaining the highest instrument sensitivity. The increased instrument sensitivity will allow the instrument to reach it's full potential in determining single particle optical properties.

4 CONCLUSIONS

Two examples of the application of optimal estimation are given. The Aerosol refractive index of Cape Verde dust has been successfully retrieved. The method is unique as it provides spectrally resolved refractive index data from a real aerosol, current published measurements have only been made on bulk samples. This work is soon to be expanded to include black-carbon aerosol. This will allow the investigation of the applicability of the widely used of mie theory, which assumes spherical particles to predict the radiative forcing of this aerosol type despite it being far from spherical. A novel method to determine individual particle refractive index has been described, and this is very much work in progress (subject to funding). The method shows potential to determine single scatter albedo, particle refractive index and size on individual particles for the first time. These new methods show great potential in characterisation of transport particulate (in particular black carbon) emissions from transport sources both in the field and for laboratory studies.

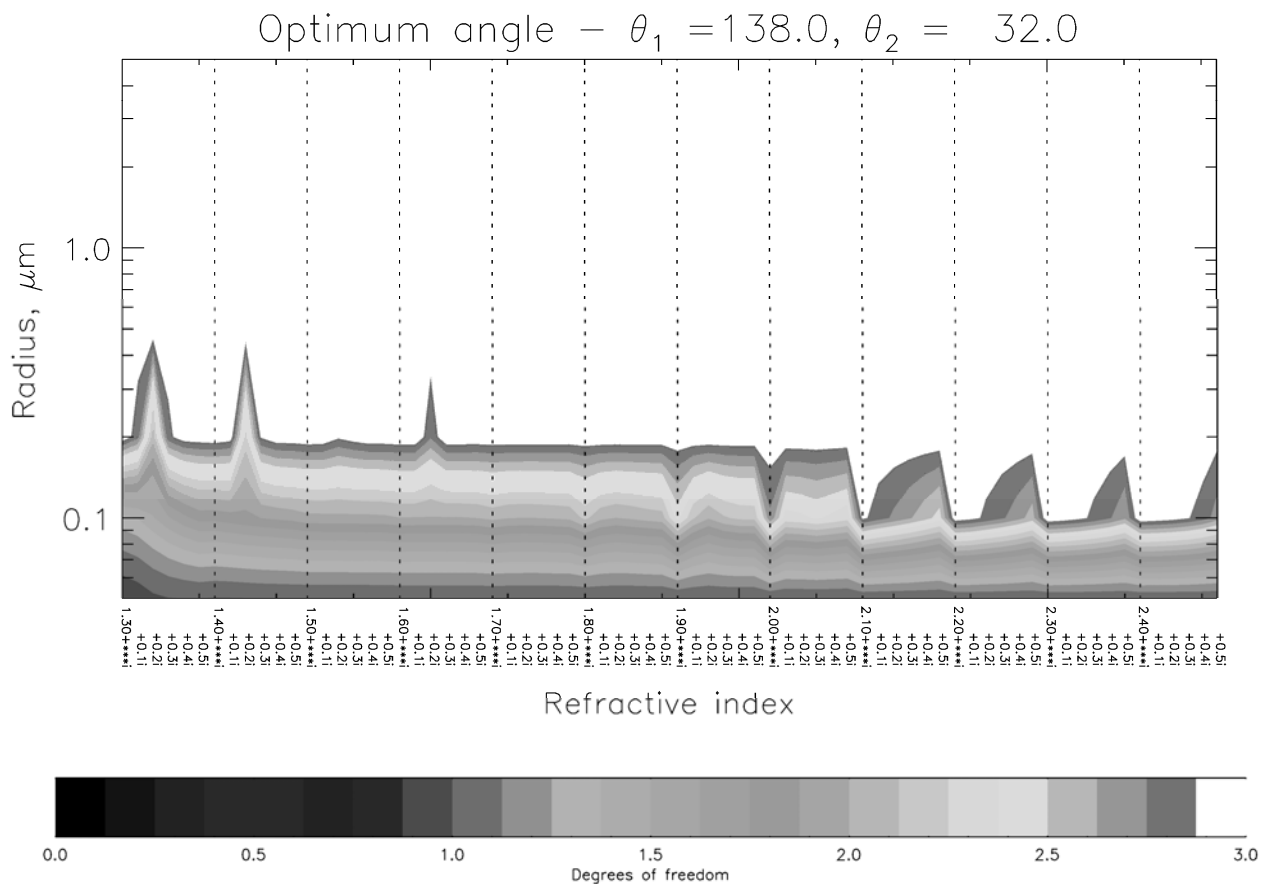


Figure 4. Optimal instrument calculated performance.

REFERENCES

- Dashler T., et al., 2003, Thirty years of in situ stratospheric aerosol size distribution measurements from laramie, wyoming (41°n), using balloonborne instruments. *J. Geophys. Res.*, 104, D5, 4167
- Shettle E.P. and Fenn .R.W. 1979 Models for the aerosols of the lower atmosphere and the effects of humidity variations on their optical properties. Technical Report AFGL-TR-79-0214, Air Force Geophysics Laboratory
- Thomas G. E., Bass S. F., Grainger R. G., and Lambert A., 2005., Retrieval of aerosol refractive index from extinction spectra with a damped harmonic-oscillator band model. *Applied Optics*, 44, 7, 1332-1341
- Rodgers C. D., 2000: *Inverse methods for atmospheric sounding: Theory and practice Vol 2*. World scientific publishing Co., ISBN-10: 981022740X, 240 pages
- Irshad R., Grainger R. G., Peters D. M., McPheat R. A., Smith K. M., and Thomas G., 2009, Laboratory measurements of the optical properties of sea salt aerosol, *Atmos. Chem. Phys.*, 9, 221-230

Distinctive Efficacies of the Components Contributing to Total Aviation Climate Impact

M. Ponater*

Deutsches Zentrum für Luft- und Raumfahrt, Institut für Physik der Atmosphäre, Oberpfaffenhofen, Germany

Keywords: Aviation Climate Impact, Contrails, Water Vapour, Efficacy

ABSTRACT: Separate climate sensitivity simulations were run for all important non-CO₂ radiative forcing contributions from aviation (except for contrail cirrus), aiming at the quantification of an individual efficacy parameter for each component. All simulations were performed with the same climate model, E39A. The necessity to scale the original perturbations complicates a straightforward determination of efficacy values, particularly for aviation ozone. The results presented here indicate that a radiative forcing from water vapour increase caused by supersonic aviation would have a similar efficacy than CO₂. Ozone changes induced by subsonic aviation and methane changes appear to have an efficacy larger than CO₂, but the enhancement is moderate (~1.05). For line-shaped contrails we find an efficacy substantially smaller (~0.6) than CO₂ in agreement with previous results. The (small) water vapour increase expected from subsonic aviation shows reduced efficacy (~0.7), too. Similar studies with other climate models are desirable in view of probable model dependency.

1 INTRODUCTION

Aviation impacts on climate in a variety of ways. Radiatively active atmospheric trace gases are changed either directly by aircraft emissions (e.g., CO₂, water vapour) or indirectly (e.g., O₃, CH₄) if atmospheric chemistry is modified by emitting reactive components such as NO_x or aerosols. A further change of the Earth's radiative balance is caused by emissions (water vapour, aerosols) that modify cloudiness, e.g., cirrus coverage and optical properties. According to well-established IPCC practice, all these climate impact components have been compared, quantitatively, in terms of their radiative forcing (e.g., Penner et al., 1999; Lee et al., 2009). In order to account for the differential lifetime of the various tracers when assessing their integrated future impact, more sophisticated metrics such as the Global Warming Potential or the Global Temperature Potential (Fuglestad et al., 2009) have to be used which, however, are also calculated based on the radiative forcing. The fundamental role of radiative forcing (RF) originates from the empirical equation

$$\Delta T_{\text{sfc}} = \lambda \cdot \text{RF} \quad (1)$$

linking RF linearly to the equilibrium change of global mean surface temperature (ΔT_{sfc}) through an assumed constant, the climate sensitivity parameter λ . There has been mounting evidence that, in particular in case of non-homogeneous perturbations (e.g., Joshi et al., 2003), individual climate sensitivity parameters ($\lambda^{(i)}$) different from the basic climate sensitivity due to a homogeneous CO₂ increase ($\lambda^{(\text{CO}_2)}$) may emerge. Hansen et al. (2005) have proposed to define efficacy parameters ($r^{(i)}$) for such perturbations, retaining the relation given by Eq. (1) in a more comprehensive expression:

$$\Delta T_{\text{sfc}} = \lambda^{(i)} \cdot \text{RF} = r^{(i)} \cdot \lambda^{(\text{CO}_2)} \cdot \text{RF} \quad (2).$$

Hereafter we will present results from climate sensitivity simulations driven by aviation related RFs (from aviation induced ozone, methane, water vapour, contrails), in an attempt to assign unique efficacy parameters to such forcings. This extends earlier efforts (Ponater et al, 2006, 2007) that lacked consistency in the sense that results were compiled from various model systems. Here, all

* *Corresponding author:* Michael Ponater, DLR-Institut für Physik der Atmosphäre, Oberpfaffenhofen, D-82230 Wessling, Germany. Email: Michael.ponater@dlr.de

simulations have been run with the ECHAM4/ATTILA (E39A) model system described by Stenke et al. (2008). This model involves enhanced vertical resolution around the tropopause and a Lagrangian advection scheme for water vapour and cloud water which makes it especially suitable to describe forcings and feedbacks in the upper troposphere and lower stratosphere region.

2 THE SCALING PROBLEM

As shown by Lee et al. (2009), an estimate of total RF from aviation for the year 2005 conditions amounts to about 50 mW/m^2 . (Note that this value excludes contrail cirrus, for which a reliable RF best estimate has not yet been provided. Thus, this effect is not covered in the present paper either). Individual contributions to the total aviation RF remain generally lower than 30 mW/m^2 . Forcings of this magnitude are too small to cause a statistically significant temperature signal in equilibrium climate change simulations and to derive robust values of the climate sensitivity parameter and the efficacy according to Eq. (1, 2). Thus, strong scaling of respective emissions or concentration changes is unavoidable in order to ensure significant signals. Conceptually, the climate sensitivity parameters ($\lambda^{(i)}$) in Eq. (2) are expected to be independent from the magnitude of the forcing, so RF scaling ought to be a straightforward procedure. Moderate deviations from this basic assumption have been pointed out even in the CO_2 case for a number of climate models (e.g., Senior and Mitchell, 2000; Boer and Yu, 2003; Hansen et al., 2005). Nevertheless, calculation and attribution of distinctive efficacies $r^{(i)}$ remains possible as long as their deviation from unity is sufficiently large to neglect a small uncertainty in $\lambda^{(\text{CO}_2)}$. Indeed, Hansen et al. (2005) defined $\lambda^{(\text{CO}_2)}$ with respect to a 50% CO_2 increase over a (pre-industrial) background concentration of 291 ppmv as their reference, paying little heed to the magnitude deviation of some other forcings when interpreting their efficacy values for a larger number of effects. In agreement with previous results, the E39A model used for the simulations reported hereafter shows a relatively small variability of $\lambda^{(\text{CO}_2)}$ with increasing RF: Its value is 0.70, 0.72, and 0.74 K/Wm^{-2} as $\text{RF}(\text{CO}_2)$ increases from 1.01 over 3.79 to 6.16 W/m^2 .

However, as pointed out in a companion study to the present paper (Ponater et al., this volume), it is not guaranteed that such robustness of λ exists for other forcing agents as well. Equilibrium climate change simulations with E39A, forced by ozone change patterns resulting from transport emissions, yielded a climate sensitivity increase of up to 30 % for the same pattern if the forcing was heavily scaled. Hence, in that case the efficacy proved to be more dependent on the scaling of a pattern than on its structure. While the problem could be solved by diagnostic analysis and more simulations, the respective experience suggests to limit the amount of scaling, keeping the RF at values around 1 W/m^2 (or smaller). A less welcome side effect of this decision to restrict the scaling factors is that the regression method for deriving the RF and the climate sensitivity (Gregory et al., 2004; Hansen et al., 2005) can no longer be applied due to an insufficient signal to noise ratio. However, it will be shown here that useful results can be obtained on the basis of the classical IPCC definition of RF (stratosphere adjusted radiative forcing) and the associated $\lambda^{(i)}$, and $r^{(i)}$ values.

3 RESULTS

3.1 Simulation dedicated to individual aviation forcing components

Table 1 lists the relevant parameters for each simulation run with the E39A climate model for this study. The climate sensitivity of a CO_2 increase by 72.3 ppmv (yielding about 1 W/m^2 radiative forcing) is used as a reference, as in the simulations dedicated to methane increase, aviation water vapour increase, and contrails forcings were scaled to a similar magnitude. Note that this means a slight deviation from the way the CO_2 reference value was reached in the companion study dealing with transport related ozone increase (Ponater et al., this volume). The difference is insignificant, however: The climate sensitivity of a 1 W/m^2 CO_2 radiative forcing results as 0.696 K/Wm^{-2} with an estimated 95 % confidence interval of 0.02 K/Wm^{-2} , while the climate sensitivity of CO_2 approximated via the nonlinear fit applied in that companion study is 0.692 K/Wm^{-2} . We further recall that the efficacy of aviation ozone according to Ponater et al., this volume, is about 1.05. This is close to the values directly derived from the two aviation ozone simulations (O3 and O4, using a scaling factor of 50 and 100, respectively) as given Table 1.

	RF_{adj}	ΔT_{sfc}	λ_{adj}	ϵ_{adj}
CO ₂ (1 W/m ²)	1.010	0.703	0.696	1
OZavi (30) – O1	0.540	-	-	-
OZavi (40) – O2	0.704	-	-	-
OZavi (50) – O3	0.862	0.617	0.712	1.02
OZavi (100) – O4	1.593	1.167	0.733	1.05
CH ₄ (1 W/m ²)	1.053	0.760	0.722	1.04
CH ₄ (2 W/m ²)	2.123	1.576	0.742	1.07
Contrails (80, $\tau=0.3$) – C1	0.609	-	-	-
Contrails (80, $\tau=0.4$) – C2	0.833	0.385	0.462	0.66
Contrails (100, $\tau=0.3$) – C3	0.694	0.297	0.427	0.61
Contrails (100, $\tau=0.4$) – C4	0.928	0.383	0.413	0.59
WatVap_avia_sub (750) – H1	0.442	0.223	0.505	0.72
WatVap_avia_sub (1000) – H2	0.555	0.273	0.492	0.71
WatVap_avia_super (20) – HS	0.585	0.428	0.732	1.05
	[Wm ⁻²]	[K]	[K/Wm ⁻²]	

Table 1: Radiative forcing, global mean surface temperature change, climate sensitivity, and efficacy as found in equilibrium climate change simulations with the E39A model. Forcing types are a homogeneous CO₂ increase, the aviation ozone change pattern (OZavi) as given by Hoor et al. (2009), scaled by various factors, a homogeneous CH₄ increase, scaled contrails, and two patterns of aviation induced water vapour increase (see text). In case of the O1, O2, and C1 perturbations, only the stratosphere adjusted radiative forcing (RF_{adj}) was calculated.

Two simulations were performed with two different amounts of homogeneous CH₄ concentration increase to yield either about 1 W/m² (+3.11 ppmv) or about 2 W/m² (+8.6 ppmv) radiative forcing, respectively. Similar to the CO₂ case, the climate sensitivity of a methane perturbation shows only little dependency on the scaling. The moderate efficacy enhancement of CH₄ versus CO₂ changes is consistent with results reported by Hansen et al. (2005), but there have also been examples of climate models with a CH₄ efficacy smaller than that of CO₂ (Berntsen et al., 2005).

When based on a realistic air traffic density, line-shaped contrails provide only a small radiative forcing (< 15 mW/m²), hence their amount must be scaled substantially. In the only study that has attempted to estimate an efficacy of contrail forcing before (Ponater et al., 2005), a 2050 aviation inventory was scaled by a factor 20, still yielding a radiative forcing as low as 0.2 W/m². In that study the contrail optical depth was not scaled, rather the varying optical depth values (yielding a mean around 0.1) from the contrail parameterisation scheme of Ponater et al. (2002) were retained. This resulted in a marginally significant surface temperature response just sufficient for the purpose of deriving an interpretable efficacy change. Even higher scaling of air traffic density can hardly be recommended, as the contrail coverage pattern may be influenced by excessive scaling as soon as saturation effects for certain regions show up. Hence, for the contrail simulations discussed in this study (Table 1) we decided to scale both air traffic density (contrail coverage) and contrail optical depth in order to reach a larger global contrail radiative forcing around 1 W/m². The basic inventory was the same as in Ponater et al. (2002), referring to 1992 aviation density, which was scaled by factors of 80 or 100, while contrail optical depth τ was prescribed to a uniform value of 0.3 or 0.4.

The three contrail driven equilibrium climate change simulations C2, C3, and C4 (Table 1), slightly varying with respect to the choice of scaling, all indicated a similar climate sensitivity parameter around 0.45 K/Wm⁻², suggesting that the resulting efficacy of about 0.6 has some degree of robustness. The value also agrees with the one estimated by Ponater et al. (2005) with a (slightly) different climate model and, as explained above, a somewhat different simulation setup. In view of the higher degree of model dependency for the efficacy parameter that has been found in studies dealing with, e.g., ozone change patterns (Joshi et al., 2003; Berntsen et al., 2005), the indications for a substantially reduced efficacy of contrails are strong indeed.

Two simulations for the present study (H1, H2, Table 1) were dedicated to the water vapour change induced by subsonic aviation. The respective concentration increase pattern is characterised by a distinct maximum in the northern hemisphere lowermost stratosphere (Ponater et al., 2006, their Fig. 3). Typical radiative forcings of a perturbation of this magnitude are very small (below 2 mW/m² for present day aviation, Lee et al., 2009), and a large scaling has to be applied in order to increase the respective response in equilibrium climate change simulations to acceptable levels of statistical significance. The simulations H1 and H2 consistently suggest an efficacy substantially

smaller than the CO₂ reference for this type of forcing. The estimated value is about 0.7, which does not agree with the efficacy suggested in Ponater et al. (2006) for aviation water vapour (1.14). The latter value was, however, derived from a water vapour concentration change pattern induced by a hypothetical supersonic air fleet in the stratosphere (Søvde et al., 2007), which is characterised by a different structure and a much higher basic radiative forcing of around 35 mW/m² (Myhre et al., 2009). In order to confirm whether the different concentration change pattern causes the difference in efficacies we repeated with E39A the simulation forced by the supersonic aviation water vapour increase scaled with a factor 20 (HS, Table 1). The respective efficacy parameter is 1.05, which is hardly distinguishable from 1 in a statistical sense, given the relatively small forcing of 0.585 W/m².

Summarizing, there are at least two contributions to aircraft climate impact whose forcing may be associated with an efficacy significantly different from unity, line-shaped contrails and water vapour induced by subsonic aviation.

3.2 Simulations dedicated to forcings from combined individual components

The usefulness of introducing distinctive efficacies in assessment studies would greatly increase if they can serve as linear weighting factors in case that the response to a combined perturbation (e.g., aviation total impact) is to be derived from the individual response components.

$$\Delta T_{\text{sfc,comb}} = r_{\text{comb}} \cdot \lambda^{(\text{CO}_2)} \cdot \text{RF}_{\text{comb}} \quad ; \quad r_{\text{comb}} = \frac{\sum(\text{RF}^{(i)} \cdot r^{(i)})}{\sum \text{RF}^{(i)}} \quad ; \quad \text{RF}_{\text{comb}} = \sum \text{RF}^{(i)} \quad (3)$$

This possibility was explored by some simulations forced by more than one of the individual impact contributions (Table 2). Our guideline in choosing appropriate combinations has been not to diverge too far from the standard. For this purpose perturbations with smaller forcing had to be employed (O1, O2, C1, Table 1), for which no dedicated efficacy values from individual simulations had been determined. However, this investigation was built on the hypothesis of unique efficacies for each component anyway, which were assumed according to the last section: 1.05 for water vapour from supersonics and ozone, 0.6 for contrails, and 0.7 for water vapour from subsonics.

	RF _{adj}	ΔT _{sfc}	λ _{adj}	r _{adj}	r _{adj} (comb)
CO ₂ (1 W/m ²)	1.010	0.703	0.696	1	-
O1 + C1	1.122 (98%)	0.683	0.609	0.86	0.83
O2 + C3	1.409 (100%)	0.854	0.606	0.87	0.82
O1 + H1	0.983 (100%)	0.609	0.620	0.89	0.89
O2 + HS	1.294 (100%)	0.994	0.768	1.10	1.05
C1 + H1	1.037 (98%)	0.494	0.476	0.68	0.65
C1 + HS	1.201 (100%)	0.716	0.596	0.86	0.82
C1 + O1 + H1	1.577 (99%)	0.935	0.593	0.85	0.79
	[Wm ⁻²]	[K]	[K/Wm ⁻²]		

Table 2: Radiative Forcing, surface temperature response, climate sensitivity, and efficacy of simulations using more than one aviation impact components. The designations in the 1st column refer to aviation ozone (O), contrail (C), and aviation water vapour (H) perturbations, whose individual forcing and response parameters are given in Table 1. 4th column is the efficacy derived from the actual λ_{adj} values, 5th column the efficacy reached through linear combination according to Equation 3 (see text).

Going through Table 2 it can be noted first (2nd column) that the contributing radiative forcings are almost perfectly additive, a necessary precondition for the linearization of efficacies (Eq. 3) to work. Second, the efficacy parameter for the combined perturbation always takes a value between the contributing component efficacies, except for “O2+HS”, where both component efficacies are assumed as equal (1.05) and should also be equal to the combined efficacy in an ideal case. However, as all efficacy parameter values are subject to a statistical uncertainty (which I do not give here due to lack of space), this is still an acceptable degree of non-linearity. The efficacy parameter of a combined perturbation calculated by linear combination of the contributing individual efficacy values (Table 2, last column) are close to the efficacy parameters from the actual climate model simulations forced by the combined perturbation, but with a tendency towards underestimation. This can be related to the fact that the simulations driven by the combined perturbations have, in general, larger forcings. As we already know, for most perturbations larger forcing inhibits higher efficacy. All in all, deviations from the linearity concept behind Eq. 1 to 3 appear to be limited for radiative forcings below 1.5 W/m². This provides some confidence in using individual efficacies as

weighting factors when the respective perturbations and forcings are combined. The method should be suitable even more so for assessing the present-day aviation climate impact.

4 DISCUSSION AND CONCLUSIONS

Evidence of a distinctive efficacy for at least some individual aviation forcing components poses the question, which feedback mechanisms are at the root of such anomalous effects. The reasons may be different from perturbation to perturbation and also different from model to model. This paper restricts to a brief look at the contrail case, for which the efficacy deviates strongest from the CO₂ reference. As mentioned, Ponater et al. (2005) found a quantitatively similar efficacy reduction for contrails in a previous version of the climate model applied here. Their explanation was, that due to the absence of contrail radiative forcing over the Arctic (where there is only little air traffic) the temperature response at these latitudes is weakened. This entails reduced ice-albedo feedback and reduced global climate sensitivity. The same effect is also apparent, but to a less extent, in the E39A simulations presented here (not shown). Further analysis reveals, however, that the radiative feedback of natural clouds to a contrail forcing also significantly deviates in comparison to a respective CO₂ driven simulation.

	λ_{adj}	$\Delta\text{CRF}(\text{sw})$	$\Delta\text{CRF}(\text{lw})$	ΔCRF	$\Delta\text{CRF}/\Delta T_{\text{surf}}$
CO ₂ (1 Wm ⁻²)	0.696	-0.659	+0.532	-0.127	-0.181
Contrails (80, $\tau=0.4$) – C2	0.462	-0.296	-0.058	-0.354	-0.919
Contrails (100, $\tau=0.3$) – C3	0.423	-0.262	-0.111	-0.373	-1.255
Contrails (100, $\tau=0.4$) – C4	0.413	-0.365	-0.110	-0.475	-1.240
	[K/Wm ⁻²]	[Wm ⁻²]	[Wm ⁻²]	[Wm ⁻²]	[Wm ⁻² /K]

Table 3: Climate sensitivity, shortwave, longwave, and net radiative feedbacks of natural clouds, and the specific net cloud feedback for the E39A equilibrium climate change simulations driven by CO₂ increase and by scaled forcing of line-shaped contrails (see text). The corresponding global mean surface temperature response can be found in Table 1. The radiative feedback of natural clouds has been taken as the difference of the radiative forcing of natural clouds between the respective simulation and the control simulation.

Table 3 presents the radiative feedback related to changes in natural cloudiness for the three contrail simulations already discussed in Section 3.1, together with the CO₂ increase simulation scaled to 1 W/m² forcing. The latter exhibits negative cloud feedback in the solar spectrum (i.e., enhanced shortwave cooling) and positive cloud feedback in the terrestrial spectrum (i.e., enhanced longwave warming) yielding a comparatively small net cooling effect. In the contrail driven simulations both shortwave and longwave feedback components are negative, resulting in a stronger negative net feedback. It is notable that in simulations C2, C3, and C4 natural cirrus cloud coverage decreases at latitudes and altitudes where contrails are present, while in the CO₂ driven simulation cirrus cloud coverage increases in the same regions (not shown). As natural cirrus clouds provide a warming of the climate system it is consistent that the climate sensitivity of a perturbation should be reduced if it acts to remove cirrus coverage. The contrails produced by the parameterisation of Ponater et al. (2002) warm the upper troposphere and reduce the relative humidity, which could easily lead to the effect that they offset part of their own positive radiative forcing by allowing less natural cirrus than in an atmosphere without contrails. Whether this is an effect reflecting the role of contrails in the real world correctly must remain an open question at this stage.

It can be concluded that efficacy anomalies for some individual effects of aircraft total climate impact are significant, require further research, and deserve attention when determining the balance of effects in aviation assessment studies. Respective indications are obvious for contrails and should be taken into consideration in forthcoming studies of contrail cirrus (see Burkhardt et al., 2010), as its presumably higher radiative forcing makes knowledge of its efficacy even more relevant. The simulations presented here and in the dedicated paper of Ponater et al., this volume, do not confirm the distinct efficacy increase suggested for aviation ozone by previous studies that used idealized ozone change patterns in extra-tropical latitudes (e.g., Stuber et al., 2005). For all aviation impact components more model studies are clearly required in order to allow more reliable conclusions.

ACKNOWLEDGEMENTS:

This study was funded within the QUANTIFY project supported by the European Union within the 6th Framework Project under contract 003893.

REFERENCES

- Berntsen, T., J. Fuglestvedt, M. Joshi, K.P. Shine, N. Stuber, M. Ponater, R. Sausen, D.A. Hauglustaine, and L. Li, 2010: Response of climate to regional emissions of ozone precursors: sensitivities and warming potentials, *Tellus* 57B, 283-304.
- Burkhardt, U., B. Kärcher, and U. Schumann, 2010: Global modelling of contrail and contrail cirrus climate impact, *Bull. Am. Meteorol. Soc.*, in press.
- Boer, G.J. and B. Yu, 2003: Climate sensitivity and climate state, *Clim. Dyn.* 21, 167-176, doi: 10.1007/s00382-003-0323-7.
- Fuglestvedt, J., et al., 2009: Transport impacts on atmosphere and climate: Metrics, *Atmos. Environ.*, in press, doi: 10.1016/j.atmosenv.2009.04.044.
- Gregory, J., et al., 2004: A new method diagnosing radiative forcing and climate sensitivity. *Geophys. Res. Lett.* 31, L03205, doi:10.1029/2003GL018747.
- Hansen, J., M. Sato, R. Ruedy, L. Nazarenko, A. Lacis, G.A. Schmidt, G. Russell, et al., 2005: Efficacy of climate forcings. *J. Geophys. Res.* 110, D18104, doi: 10.1029/2005GL022740.
- Hoor P., et al., 2009: The impact of traffic emissions on atmospheric ozone and OH: results from QUANTIFY. *Atmos. Chem. Phys.* 9, 3113-3136.
- Joshi, M., K.P. Shine, M. Ponater, N. Stuber, R. Sausen, and L. Li, 2003: A comparison of climate response to different radiative forcings in three general circulation models: towards an improved metric of climate change. *Clim. Dyn.* 20, 843-854, doi: 10.1007/s00382-003-0305-9.
- Lee, D.S., D.W. Fahey, P.M. Forster, P.J. Newton, R.C.N. Wit, L.L. Lim, B. Owen, R. Sausen, 2009: Aviation and global climate change in the 21st century, *Atmos. Environ.* 43, 3520-3537.
- Myhre, G., et al., 2009: Intercomparison of radiative forcing calculations of stratospheric water vapour and contrails. *Meteorol. Z.* 18, 585-596, doi: 10.1127/0941-2948/2009/0411.
- Penner, J., D.H. Lister, D.J. Griggs, D.J. Dokken, M. McFarland (Eds.), 1999: Aviation and the Global Atmosphere, Special Report of the Intergovernmental Panel on Climate Change, Cambridge Univ. Press, 365pp.
- Ponater, M., S. Marquart, R. Sausen, 2002: Contrails in a comprehensive global climate model: Parameterisation and radiative forcing results. *J. Geophys. Res.* 107, 4164, doi:10.1029/2005JD22580.
- Ponater, M., S. Marquart, R. Sausen, U. Schumann, 2005: On Contrail Climate Sensitivity. *Geophys. Res. Lett.* 32, L10706, doi:10.1029/2005GL22580.
- Ponater, M., S. Pechtl, R. Sausen, U. Schumann, G. Hüttig, 2006: Potential of the cryoplane technology to reduce aircraft climate impact: A state of the art assessment. *Atmos. Environ.* 40, 6928-6944, doi:10.1016/j.atmosenv.2006.06.036.
- Ponater, M., V. Grewe, R. Sausen, U. Schumann, S. Pechtl, E.J. Highwood, N. Stuber, 2007: Climate sensitivity of radiative impacts from transport systems. In: *Proceedings of an International Conference on Transport, Atmosphere and Climate (TAC)* (Eds. R. Sausen et al.), European Communities, Oberpfaffenhofen, Germany, 320pp.
- Shine, K.P., et al., 1990: Radiative forcing of climate. In: *Climate change: The IPCC scientific assessment* (Eds.: Houghton, J.T., et al.), Cambridge University Press, Cambridge, New York, Melbourne, Sydney.
- Stenke, A., V. Grewe, V., M. Ponater, 2008: Lagrangian transport of water vapour and cloud water in the ECHAM4 GCM and impact on the cold bias. *Clim. Dyn.*, 31, 491-506, doi: 10.1007/s00382-007-0347-5.
- Stuber, N., M. Ponater, and R. Sausen, 2005: Why radiative forcing might fail as a predictor of climate change. *Clim. Dyn.* 24, 497-510, doi:10-1007/s00382-004-0497-7.
- Senior, C.A., and J.F.B. Mitchell, 2000: The time dependence of climate sensitivity. *Geophys. Res. Lett.* 27, 2685-2689.
- Søvde, O.A., M. Gauss, I.S.A. Isaksen, G. Pitari, and C. Marizy, 2007: Aircraft pollution – a futuristic view. *Atmos. Chem. Phys.* 7, 3621-3632.

Aviation NO_x Global Warming Potential

Agnieszka Skowron^{*}, David S. Lee, Jane Hurley

Dalton Research Institute, Manchester Metropolitan University, John Dalton Building, Chester Street, Manchester, M1 5GD, United Kingdom

Keywords: GWP, aviation NO_x emissions, O₃ non-linearity

ABSTRACT: The dual approach of using 2D and 3D Chemical Transport Models (CTMs) was adopted to deal with the temporal discrepancies of aircraft O₃ and CH₄ responses. A series of pulse and sustained experiments over 100-year horizons of aircraft O₃ and CH₄ for a range of aviation NO_x emission rates were carried out. Observed at a global scale, the non-linear aircraft O₃ response with respect to aircraft NO_x emissions rates may hold the key for understanding the discrepancy between reported aviation NO_x GWPs.

1 INTRODUCTION

The Global Warming Potential (GWP), since it was introduced at the first Intergovernmental Panel on Climate Change (IPCC) scientific assessment in 1990 (IPCC, 1990) became widely and deeply accepted as an appropriate measure by the user community. Usage of the GWP is the established method for comparing the potential impact of emissions of different long-lived greenhouse gases on climate under the Kyoto Protocol. A GWP is defined as the integrated radiative forcing from a unit emission of a gas over a certain defined time horizon relative to the unit emission of a reference gas (by convention, CO₂) over the same time horizon. The GWP places emissions of gases with different lifetimes and radiative properties on a common scale. This leads to weaknesses and uncertainties (Smith and Wigley, 2000a, b; Fuglestedt et al., 2003; Shine et al., 2005a, b, 2007), which are challenges particularly for short-lived species and their precursors, e.g. the aviation NO_x emissions (IPCC, 1999).

The coupled NO_x-O₃-CH₄ system, as affected by aviation NO_x emissions, results in a short-term O₃ positive radiative forcing and a long-term O₃ and CH₄ negative responses. Nonetheless the overall radiative forcing induced by current day emissions of aviation NO_x is positive (Lee et al., 2009). These processes act on different spatial and temporal scales, which is why defining a unanimous result describing the impact of aviation NO_x on climate remains challenging and controversial.

IPCC AR4 WGI recently summarized studies that attempted to define an aviation NO_x GWP (Forster et al., 2007). Only three studies were identified, which yielded NO_x GWPs for aviation of: 100 (Derwent et al., 2001), 130 (Wild et al., 2001), and -3 (Stevenson et al., 2004). In addition, a recent study of Köhler et al. (2008) produced aviation NO_x GWP of 68. These GWPs have recently been re-evaluated by Fuglestedt et al. (2009), yielding values of -2.1, 71, 6.9.

Such a wide range of results make it difficult to recommend an aviation NO_x GWP for formulating policy (Faber et al., 2008). These few and disparate values of aviation NO_x GWP are the motivation of this study, in which a preliminary attempt of unravelling these apparent disagreements is presented.

2 METHODOLOGY

One of the fundamental difficulties in calculating a GWP for aviation NO_x is that the timescales of responses of O₃ enhancement and CH₄ depletion are very different, such that the CH₄ results are often parameterized rather than fully calculated, since long integration times of the order of several

^{*} *Corresponding author:* A. Skowron, Dalton Research Institute-CATE, Manchester Metropolitan University, Faculty of Science and Engineering, John Dalton Building, Chester St, Manchester M1 5GD, UK. Email: a.skowron@mmu.ac.uk

CH₄ lifetimes (~ 8 – 10 years) are required – and such simulations are computationally expensive. We adopt a dual approach of using 2D and 3D CTMs to deal with the temporal discrepancies of responses.

The Two-dimensional Chemistry Model (TROPOS) is a latitudinally-averaged two-dimensional Eulerian global tropospheric chemistry model (Hough, 1989, 1991), with a domain which extends from pole-to-pole (24 latitudinal grid cells) and from the surface to an altitude of 24 km (12 vertical layers). TROPOS is driven by chemistry, emissions, transport, removal processes and upper boundary conditions. The revised values of emissions, thermal and photolysis reactions rates, cross-sections and quantum yield are applied and based on recent evaluations. This 2D CTM has the disadvantage of not fully representing atmospheric transport, but has the advantage of a complex chemical scheme and being computationally efficient such that many long-term integrations (of the order of 100 years) are easily achieved.

The Model for Ozone and Related Tracers, version 2 (MOZART-2) (Horowitz et al., 2003) is a state-of-the-art global 3D CTM. The model has been used at a T63LR resolution (~ 1.875° x 1.875°) and has a vertical domain of 47 layers which extends upward to around 10 hPa. The chemical scheme provides a detailed study of the distribution and budget of tropospheric ozone and its precursors. MOZART-2 is driven by meteorological fields from the European Centre for Medium Range Weather Forecasting (ECMWF), with schemes accounting for dynamical and removal processes, emissions, as well as boundary layer parameterizations.

Qualitative comparisons between basic characteristics of ozone precursor distributions produced from MOZART-2 (as a 3D CTM) and TROPOS (2D CTM) simulations were used to justify employing TROPOS to carry out long-term simulations, as TROPOS is capable of reproducing many of the broad-scale features simulated by the more-complete MOZART-2 model. Thus, it was possible to run TROPOS simulations for many perturbations of different magnitudes and natures. The series of pulse and sustained experiments over 100 year horizons of aircraft O₃ and CH₄ for a range of aviation NO_x rates were calculated.

All TROPOS integrations were run for a 103 years, where the ‘spin-up’ constitutes the first two years, beginning at January 2000 from realistic initializations. The sustained aviation simulation, with aircraft emissions of 2.8 Tg NO₂, was differenced against to the base case (without aircraft). The pulse emission experiments, on the other hand, had pulses applied globally for a period of a year during the third year of simulation, having aircraft emission rates ranging from 1.0 to 5.0 Tg N. A simulation having 2.8 Tg of aviation NO₂ (0.85 Tg N) is taken to be the base case for each pulse size.

3 RESULTS AND DISCUSSION

In all cases, the positive short-term O₃, negative long-term CH₄ and negative long-term O₃ responses were observed, the different shapes and magnitudes of behaviour reflect the varying natures of the individual experiments.

3.1 TROPOS vs MOZART-2

The 2D CTM reliability was justified with 3D CTM results. Figure 1 presents the distributions (latitude vs altitude) of O₃ and CH₄. A good agreement between these two models in terms of absolute and aircraft perturbation patterns is observed.

The largest mixing ratios of O₃ occur around the 20 km, where the photolysis of molecular oxygen is more intensive than in the lower parts of the atmosphere. The CH₄ distribution follows the emission sources, which explains the maximum in number densities observed at mid-to-high latitudes of the Northern Hemisphere (where the higher emission rates occur). This maximum in CH₄ is compounded by the fact that the removal of CH₄ by OH is slower in the mid-to-high latitudes, than in the tropics because of the temperature dependence of CH₄+OH reaction.

The aircraft perturbation distributions display well-known patterns. Aviation NO_x results in an increase in O₃ concentration. This response is observed mainly in the air traffic corridors, as O₃ is rather short-lived, with its lifetime of weeks. The increased concentrations of OH, caused by the O₃ enhancement, act to remove CH₄ from the atmosphere (the CH₄+OH reaction is the main removal path for tropospheric CH₄). The CH₄ is well-mixed through the globe, due to its long lifetime,

which is why its observed decline is distributed globally.

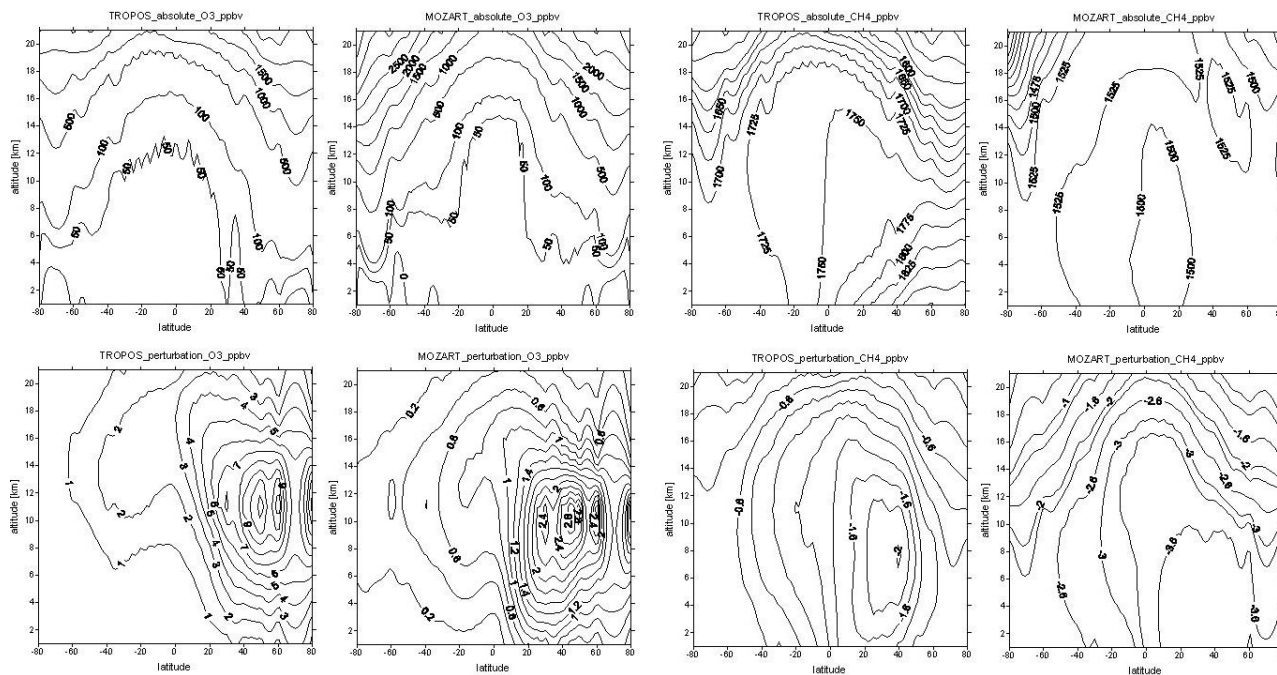


Figure 1: The distribution (latitude vs altitude) of O₃ and CH₄ (respectively from left to right) for absolute (first row) and aircraft perturbation (second row) values in TROPOS and MOZART-2. The pattern of aircraft O₃ perturbation is in good agreement between the 2D and 3D simulations, despite the fact that O₃ production from aviation NO_x seems to be more efficient in TROPOS (higher maximum values). This can be explained by the 2D model shortcomings – for example, too coarse a spatial resolution can result in the transport of NO_x into remote environments and hence O₃ production in these NO_x-limited environments (Johnson and Derwent, 1996; Derwent et al., 2001).

The 2D CTM results were also compared with measurements. As most of the experiments in this study are designed as a long-term simulations, it is important to know how well TROPOS is able to represent the variability of species, especially methane (a well-mixed gas of lifetime = ~ 10.05 years in TROPOS), over decades. Figure 2 presents the modelled methane volume mixing ratios from the two lowest layers for three chosen latitude bands as compared with the observations of Dlugokencky et al. (2003) during the period 1983–2007. The values represent the monthly means and multiple observation points were included to show the variability within each latitude band. There is a good agreement between model and observational shapes, magnitudes and phases of the seasonal variations of methane concentrations; also the growth rate with time is well represented. While in the Southern Hemisphere the first and second of the model layers are overlapped, in the Northern Hemisphere some disparities are noticed. This is mainly due to the surface methane emissions, whose main sources occur in the northern latitudes (emissions are immediately mixed through the model surface grid cells, while in reality it takes a finite time to distribute around the latitude circle (Hough, 1991)), as well as by the fact that the air is mixed much better at the southern, especially high, latitudes.

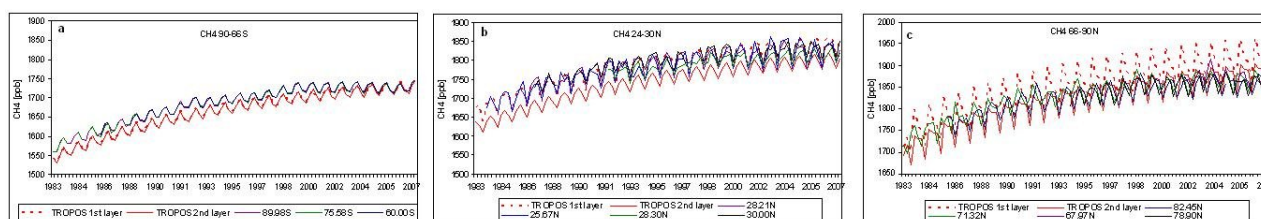


Figure 2: TROPOS vs measurements from Dlugokencky et al. (2003): the temporal variation of methane mixing ratio at chosen sites of the world. The dashed red curve is the model surface layer; the solid red curve is the model second layer. The sites are: (a) South Pole, Antarctica, 89.98°S; Halley Station, Antarctica, 75.58°S; Syowa Station, Antarctica, 69.00°S, (b) Sand Island, Midway; 28.21°N; Key Biscayne, Florida; 25.67°N; Tenerife, Canary Islands; 28.30°N; Pacific Ocean; 30.00°N, (c) Pallas-Sammaltunturi, GAW Sta-

tion, 67.97°N; Barrow, Alaska, 71.32°N; Ny-Alesund, Svalbard, 78.90°N; Alert, Nunavut, 82.45°N <http://www.esrl.noaa.gov/gmd/dv/site/PAL.html>.

3.2 Sustained Simulation

Figure 3 presents the evolution of O_3 and CH_4 perturbations over 100 years from a 2.8 Tg NO_2 sustained aviation experiment from TROPOS. We can observe the positive O_3 and negative CH_4 responses. The continuous input of aviation NO_x emissions keeps the burden of O_3 at certain level; the long-term O_3 is also pronounced and it manifests as a small (~ 1.2 Tg O_3 within the 90 years) reduction in the positive aviation O_3 perturbation. The CH_4 response for constant aircraft emission is the continual decline of its tropospheric mass, until approximately the seventieth year of simulation, when CH_4 reaches its equilibrium. CH_4 , as a long-lived gas, needs a few decades (the steady reduction of ambient CH_4 takes place with a 9.9 year CH_4 perturbation lifetime) to reach steady-state, while O_3 response is ‘instantaneous’.

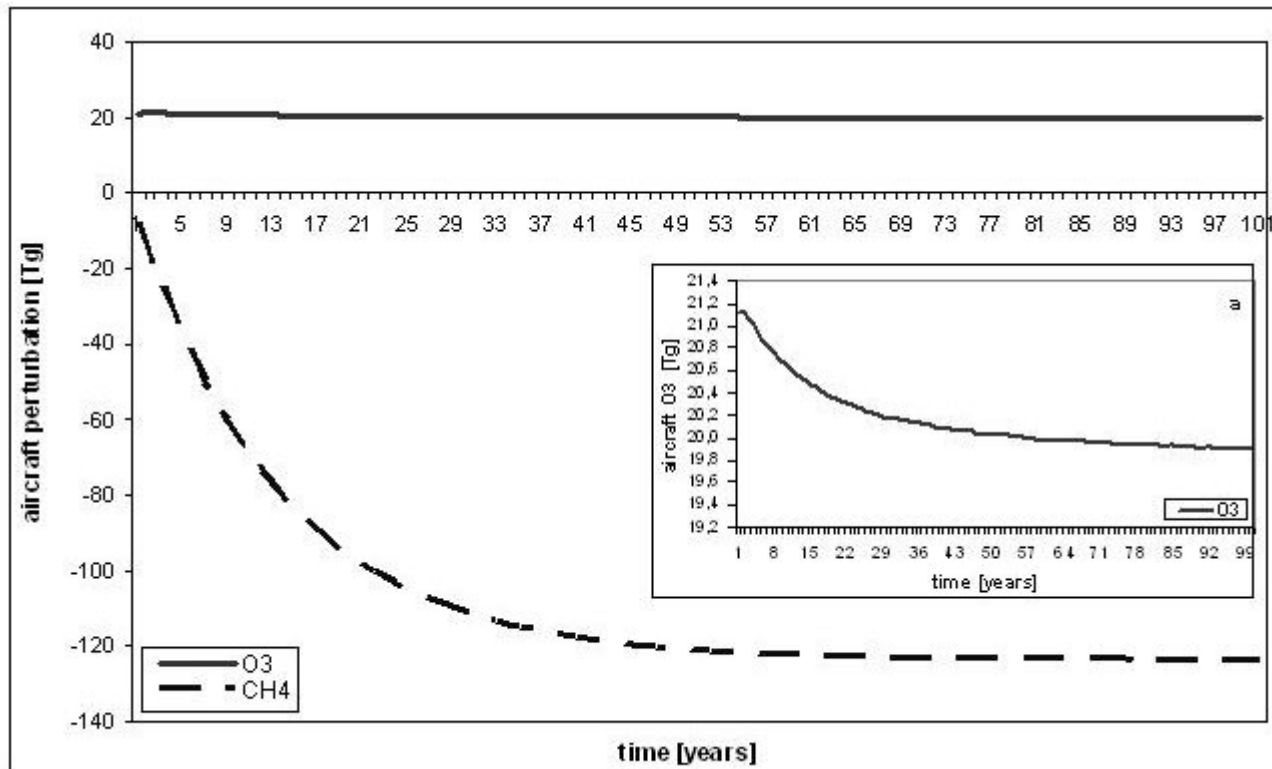


Figure 3: The time evolution of perturbations in the global burdens of ozone and methane over the 100 year horizon from the 2.8 Tg NO_2 sustained aviation experiment. The secondary O_3 is observed (a).

3.3 Pulse Simulations

Pulses are widely accepted and used to define and understand the mechanisms of complex NO_x chemistry. They are also utilized in order to assess the NO_x impact on climate through the GWP approach.

The year-long pulses are sources of easily visible short-term positive O_3 , long-term negative CH_4 and long-term negative O_3 perturbations (Fig. 4). The temporal scales of its responses are clearly shown. After each pulse, the O_3 enhancement immediately becomes noticeable, and persists for a relatively brief period, (~ 3 years); then, a year after the pulse, the negative peak response of CH_4 takes place – and, finally, at the fifth year after the pulse, the long-term negative O_3 peak response develops. It takes few decades for both CH_4 and long-term O_3 to return to their equilibrium values; the pulse size plays an important role in the length of their recovery.

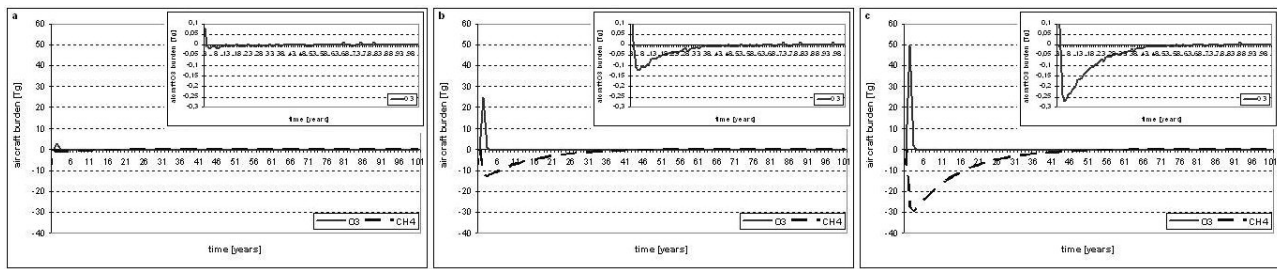


Figure 4: The time evolution of ozone and methane responses from the aircraft NO_x pulse experiments. Three different aircraft NO_x rates are presented: (a) 1.0 Tg N, (b) 2.5 Tg N, (c) 5.0 Tg N.

It is immediately visible how, with increasing rates of emission of aviation NO_x, the methane response increasingly dominates over the positive O₃ perturbation. The proportion of O₃ burden to CH₄ burden decreases with higher NO_x: for 1.0 Tg N, the O₃ burden constitute 14.5% of the CH₄ perturbation, whilst for 2.5 Tg N and 5.0 Tg N, it falls to 12.7% and 11.1% of the CH₄ response, respectively. The integrated burden of CH₄ becomes more pronounced than that of O₃. The ‘production’ of O₃ seems to saturate with respect to NO_x.

The positive O₃ response weakens with larger aircraft NO_x perturbations. This leads to a non-linear behaviour of aviation O₃, which is presented in Figure 5. Previously, mainly linear characteristics of O₃ for a various aircraft emissions were shown (Grewe et al., 1999; IPCC, 1999; Köhler et al., 2008). The non-linear response is expected from the chemistry (Lin et al., 1988; Berntsen et al., 2005), but it has not been demonstrated so clearly before on a global scale. While the capacity of the troposphere to generate O₃ from NO_x is gradually declining, the non-linearity of methane burden destruction is much weaker; nevertheless it is also observed.

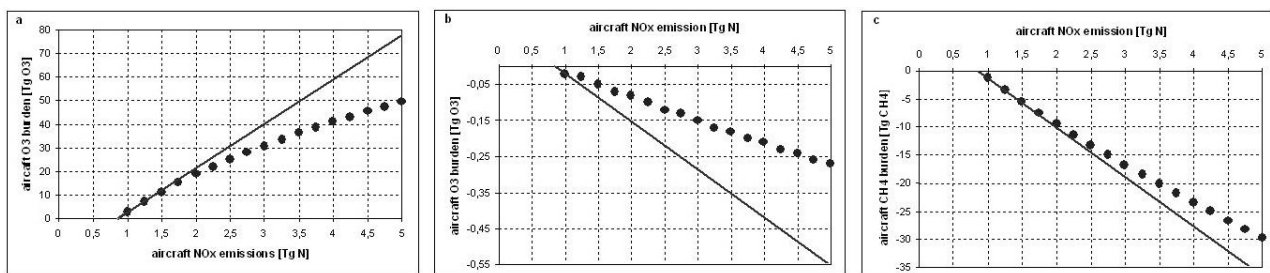


Figure 5: The modelled peak of pulse for (a) short-term O₃, (b) long-term O₃ and (c) CH₄ (dots) from a range of aircraft NO_x emissions rates. The line presents the linear solution.

4 CONCLUSIONS AND FURTHER WORK

These results imply that the O₃ response due to aircraft emissions, as observed on a global scale, is linked to the rate of emission of aircraft NO_x – and that the discrepancy between previously published NO_x GWPs may possibly be linked to the non-linear response of O₃ to aircraft NO_x emissions, particularly when the variances amongst the various experimental designs are taken into account.

These 2D CTM simulations give a unique view of NO_x chemistry perturbations, which cannot be easily achieved through 3D studies, a which long-term simulations are computationally prohibitive. It is important to carry out similar pulse experiments with a 3D CTM to confirm the results and trends suggested by this 2D CTM study.

In the next step of the work, the pulse aircraft perturbation values of O₃ and CH₄ will be translated into radiative forcings and consequently the AGWPs and GWPs will be defined for a series of aircraft NO_x rates and a range of time horizons.

REFERENCES

- Berntsen, T. K., J. S. Fuglestedt, M. M. Joshi, K. P. Shine, N. Stuber, M. Ponater, R. Sausen, D. A. Hauglustaine, and L. Li, 2005: Response of climate to regional emissions of ozone precursors: Sensitivities and warming potentials. *Tellus, Series B: Chemical and Physical Meteorology*, 57, 283-304.

- Derwent, R. G., W. J. Collins, C. E. Johnson, and D. S. Stevenson, 2001: Transient behaviour of tropospheric ozone precursors in a global 3-D CTM and their indirect greenhouse effects. *Climatic Change*, 49, 463-487.
- Dlugokencky, E. J., S. Houweling, L. Bruhwiler, K. A. Masarie, P. M. Lang, J. B. Miller and P. P. Tans, 2003: Atmospheric methane levels off: Temporary pause or a new steady-state? *Geophysical Research Letter*, 30.
- Faber, J., Greenwood, D., D. Lee, M. Mann, P. M. de Leon, D. Nelissen, B. Owen, M. Ralph, J. Tilston, A. van Velzen, G. van de Vreede, 2008: Lower NO_x at higher altitudes. Policies to reduce the climate impact of aviation NO_x emission. Delft: CE Delft.
- Forster, P., V. Ramaswamy, P. Artaxo, T. Berntsen, R. Betts, D. W. Fahey, J. Haywood, J. Lean, D. C. Lowe, G. Myhre, J. Nganga, R. Prinn, G. Raga, M. Schulz, R. Van Dorland, 2007: Changes in atmospheric constituents and in radiative forcing. In 'Climate Change', *Fourth Assessment Report of Working Group I of the Intergovernmental Panel on Climate Change*, Cambridge University Press, UK.
- Fuglestedt, J. S., T. K. Berntsen, O. Godal, R. Sausen, K. P. Shine, and T. Skodvin, 2003: Metrics of climate change: Assessing radiative forcing and emission indices. *Climatic Change*, 58, 267-331.
- Fuglestedt, J. S., K. P. Shine, T. Berntsen, J. Cook, D. S. Lee, A. Stenke, R. B. Skeie, G. J. M. Velders, and I. A. Waitz, 2009: Transport impacts on atmosphere and climate: Metrics. *Atmospheric Environment*.
- Grewe, V., M. Dameris, R. Hein, I. Köhler, and R. Sausen, 1999: Impact of future subsonic aircraft NO_x emissions on the atmospheric composition. *Geophysical Research Letters*, 26, 47-50.
- Horowitz, L. W., S. Walters, D. L. Mauzerall, L. K. Emmons, P. J. Rasch, C. Granier, X. Tie, J. F. Lamarque, M. G. Schultz, G. S. Tyndall, J. J. Orlando, and G. P. Brasseur, 2003: A global simulation of tropospheric ozone and related tracers: Description and evaluation of MOZART, version 2. *Journal of Geophysical Research D: Atmospheres*, 108.
- Hough, A. M., 1989: The development of a two-dimensional global tropospheric model. 1. The model transport. *Atmospheric Environment*, 23, 1235-1261.
- Hough, A. M., 1991: Development of a two-dimensional global tropospheric model: model chemistry. *Journal of Geophysical Research*, 96, 7325-7362.
- IPCC, 1990: *Climate Change: The Intergovernmental Panel on Climate Change*, Cambridge University Press, Cambridge, UK.
- IPCC, 1999: *Aviation and the Global Atmosphere*. J.E. Penner, D.H. Lister, D.J. Griggs, D.J. Dokken and M. McFarland (Eds). Intergovernmental Panel on Climate Change, Cambridge University Press, UK.
- Johnson, C. E. and R. G. Derwent, 1996: Relative radiative forcing consequences of global emissions of hydrocarbons, carbon monoxide and NO_x from human activities estimated with a zonally-averaged two-dimensional model. *Climatic Change*, 34, 439-462.
- Köhler, M. O., G. Rädcl, O. Dessens, K. P. Shine, H. L. Rogers, O. Wild, and J. A. Pyle, 2008: Impact of perturbations to nitrogen oxide emissions from global aviation. *Journal of Geophysical Research D: Atmospheres*, 113.
- Lee, D. S., D. W. Fahey, P. M. Forster, P. J. Newton, R. C. N. Wit, L. L. Lim, B. Owen, and R. Sausen, 2009: Aviation and global climate change in the 21st century. *Atmospheric Environment*, 43, 3520-3537.
- Lin, X., M. Trainer, and S. C. Liu, 1988: On the nonlinearity of the tropospheric ozone production. *Journal of Geophysical Research*, 93.
- Shine, K. P., J. S. Fuglestedt, K. Hailemariam, and N. Stuber, 2005a: Alternatives to the Global Warming Potential for comparing climate impacts of emissions of greenhouse gases. *Climatic Change*, 68, 281-302.
- Shine, K. P., T. K. Berntsen, J. S. Fuglestedt, and R. Sausen, 2005b: Scientific issues in the design of metrics for inclusion of oxides of nitrogen in global climate agreements. *Proceedings of the National Academy of Sciences of the United States of America*, 102, 15768-15773.
- Shine, K. P., T. K. Berntsen, J. S. Fuglestedt, R. B. Skeie, and N. Stuber, 2007: Comparing the climate effect of emissions of short- and long-lived climate agents. *Philosophical Transactions of the Royal Society A: Mathematical, Physical and Engineering Sciences*, 365, 1903-1914.
- Smith, S. J. and T. M. L. Wigley, 2000a: Global Warming Potentials: 1. Climatic implications of emissions reductions. *Climatic Change*, 44, 445-457.
- Smith, S. J. and T. M. L. Wigley, 2000b: Global Warming Potentials: 2. Accuracy. *Climatic Change*, 44, 459-469.
- Stevenson, D. S., R. M. Doherty, M. G. Sanderson, W. J. Collins, C. E. Johnson, and R. G. Derwent, 2004: Radiative forcing from aircraft NO_x emissions: Mechanisms and seasonal dependence. *Journal of Geophysical Research D: Atmospheres*, 109.
- Wild, O., M. J. Prather, and H. Akimoto, 2001: Indirect long-term global radiative cooling from NO_x emissions. *Geophysical Research Letters*, 28, 1719-1722.